New thyroid models for ICRP pediatric mesh-type reference computational phantoms

Yeon Soo Yeom [a, 1], Chansoo Choi [b, 1], Bangho Shin [b], Suhyeon Kim [b], Haegin Han [b], Sungho Moon [b], Gahee Son [b], Hyeonil Kim [b], Thang Tat Nguyen [c], Beom Sun Chung [d], Se Hyung Lee [b, e], Chan Hyeong Kim [b, *]

[a] Department of Radiation Convergence Engineering, Yonsei University, 1 Yonseidae-gil, Wonju, Gangwon-do, 26493, Republic of Korea
[b] Department of Nuclear Engineering, Hanyang University, 222 Wangsimni-ro, Seongdong-gu, Seoul, 04763, Republic of Korea
[c] School of Nuclear Engineering and Environmental Physics, Hanoi University of Science and Technology, 1 Dai Co Viet Road, Hai Ba Trung District, Hanoi, Viet Nam
[d] Department of Anatomy, Yonsei University Wonju College of Medicine, 20, Ilsan-ro, Wonju-si, Gangwon-do, 26426, Republic of Korea
[e] Department of Radiation Oncology, Bundang Jesaeng General Hospital, 20, Seohyeon-ro 180beon-gil, Bundang-gu, Seongnam-si, Gyeonggi-do, 13590, Republic of Korea

ARTICLE INFO

ABSTRACT

As part of the ICRP Task Group 103 project, we developed ten thyroid models for the pediatric mesh-type reference computational phantoms (MRCPs). The thyroid is not only a radiosensitive target organ needed for effective dose calculation but an important source region particularly for radioactive iodines. The thyroid models for the pediatric MRCPs were constructed by converting those of the pediatric voxel-type reference computational phantoms (VRCPs) in ICRP Publication 143 to a high-quality mesh format, faithfully maintaining their original topology. At the same time, we improved several anatomical parameters of the thyroid models for the pediatric MRCPs, including the mass, overlying tissue thickness, location, and isthmus dimensions. Absorbed doses to the thyroid for the pediatric MRCPs for photon external exposures were calculated and compared with those of the pediatric VRCPs, finding that the differences between the MRCPs and VRCPs were not significant except for very low energies (<0.03 MeV). Specific absorbed fractions (target ← thyroid) for photon internal exposures were also compared, where significant differences were frequently observed especially for the target organs/tissues close to the thyroid (e.g., a factor of ~1.2−~327 for the thymus as a target) due mainly to anatomical improvement of the MRCP thyroid models.

© 2022 Korean Nuclear Society, Published by Elsevier Korea LLC. This is an open access article under the CC BY license (http://creativecommons.org/licenses/by/4.0/).

1. Introduction

Recently, the International Commission on Radiological Protection (ICRP) released the pediatric voxel-type reference computational phantoms (VRCPs) in ICRP Publication 143 [1], compiling the ICRP reference phantom family with the adult VRCPs released in ICRP Publication 110 [2]. The VRCPs have been used to produce reference dose coefficients (DCs) following the current ICRP dosimetry system established in the 2007 Recommendations [3].

The voxel phantoms based on computed tomography (CT) images of the human body significantly improved the anatomy of the human body as compared with the stylized phantoms based on the mathematical equations and used for the previous ICRP dosimetry systems [4,5]. Nevertheless, the VRCPs still cannot avoid some anatomical and dosimetric limitations caused by their voxel sizes limited to a millimeter scale. The VRCPs, for example, cannot define the micron-scale target and source regions in the respiratory and alimentary tract systems established in ICRP Publications 66 and 100 [6,7]. In ICRP Publication 133 [8], the adult specific absorbed fractions (SAFs) of these organs/tissues for charged particles were calculated by using various organ/tissue-specific stylized phantoms additionally adopted instead of the adult VRCPs. The same approach is used for the pediatric SAFs being produced by the ICRP Task Group 96.

* Corresponding author. Hanyang University, 222 Wangsimni-ro, Seongdong-gu, Seoul, 04763, Republic of Korea.
E-mail address: chkim@hanyang.ac.kr (C.H. Kim).
[1] Authors who contributed equally to this work and are co-first authors of the work.

Y.S. Yeom, C. Choi, B. Shin et al.

In order to overcome the limitations of the VRCPs, the ICRP Task Group 103 was formulated with the aim of the development of new mesh-type reference computational phantoms (MRCPs) by converting the current VRCPs into a high-quality/fidelity tetrahedral mesh (TM) model [9]. The task group first developed the adult MRCPs, released in *ICRP Publication 145* [10], and is now working on the development of the pediatric MRCPs [11]. As a part of this project, the present study developed thyroid models for the pediatric MRCPs. The thyroid is radiosensitive and one of the target organs/tissues required for the calculation of effective dose [3] and also is considered an important source region particularly for internal exposure to radioactive iodines. In addition, the absorbed dose to the thyroid is considered important in radiation epidemiological studies of the thyroid cancer or other thyroid diseases [12–14]. The thyroid models of the pediatric MRCPs were converted from those of the pediatric VRCPs while the anatomy of the thyroid for each phantom was systematically revisited and improved. The dosimetric impact of the present work was also investigated by comparing thyroid DCs for several external exposures and SAFs (target ← thyroid) for photons calculated between the pediatric MRCPs and VRCPs.

2. Material and methods

2.1. Pediatric VRCPs

The pediatric VRCPs represent the Reference Male and Female at the five different ages (i.e., newborn, 1 year, 5 years, 10 years, and 15 years) [1]. For the newborn, 1-, 5-, and 10-year-old VRCPs, all organs/tissues for both male and female are identical, except for the sex-specific organs. The pediatric VRCPs were derived from corresponding pediatric phantoms developed in collaboration between the University of Florida (UF) and National Cancer Institute (NCI) [15]. The UF/NCI pediatric phantoms in the Non-Uniform Rational Basis Spline (NURBS) and polygonal mesh (PM) formats, which were constructed based on CT images, were adjusted to match the reference data (standing height, body mass, and organ/tissue masses) given in *ICRP Publication 89* [16]. The phantoms in the NURBS/PM format were then voxelized and then went through several modifications such as the inclusion of lymphatic nodes and muscle and reassignment of the organ/tissue tag numbers to be consistent with the adult VRCPs.

While the NURBS/PM modeling technique and various factors were considered in the construction of the pediatric VRCPs, there are still some anatomical limitations for the thyroid. The thyroid is located typically in front of the second and third tracheal cartilages [17,18], which anatomical feature is illustrated in Fig. 1. This typical position of the thyroid, however, was not reflected when constructing the pediatric VRCPs, and the position of thyroid of the pediatric VRCPs were largely different particularly for the newborn and 1-year-old phantoms, as shown in Fig. 2. This limitation can result in a significant bias on dose calculations particularly for internal exposures. Another limitation is seen in the overlying tissue of the thyroid, which plays an important role in thyroid dose calculations for external exposures. Table 1 compares the thyroid overlying tissue thicknesses for the pediatric VRCPs with the age-dependent typical values derived from the formula established by ultrasound measurement data of 163 Kiev inhabitants including 78 children aged from 1 to 18 years (correlation coefficient = 0.51) [19]. Note that in the present study, the overlying tissue thickness was considered the shortest distance from the skin to the thyroid. It can be seen that the thicknesses of the pediatric VRCPs are significantly different from the typical values; for example, the difference for the 1-year-old (VRCP − typical) is 18.6 mm. In addition, the typical thickness, although the degree of increase is very small,

systematically increases with the age (5.2 mm for the 1 year to 5.7 mm for the 15 years). This systematical increase, however, is not observed in the pediatric VRCPs, in which the overlying tissue for 1 year is the thickest (23.8 mm) while that for 10 years is the thinnest (0.9 mm). Lastly, the thyroid as well as other organs/tissues for the VRCPs was matched to the ICRP-89 reference values for the parenchymal organ/tissue masses, i.e., excluding the intra-organ/tissue blood masses. The thyroid should be matched to the reference organ mass inclusive of intra-organ blood.

2.2. Construction of thyroids for pediatric MRCPs

We adjusted the thyroid PM models of the UF/NCI pediatric phantoms, which are the origin of the pediatric VRCPs, by using the *Rapidform*^{TM} software (INUS Technology Inc., Korea) that provides a number of powerful tools for PM modeling [20,21]. The volume of the thyroid models was enlarged to match the reference values of the thyroid mass inclusive of the intra-organ blood mass, which are shown in Table 2. The blood-inclusive reference masses were derived using the same approach used for the adult MRCPs in ICRP *Publication 145* [10]. During the enlargement, the isthmus thickness, width, and height of the thyroid models were additionally adjusted to match the typical values determined from the literature and presented in Table 3. The isthmus thickness values for all the ages were obtained from the data established in Sea et al. [22]. The isthmus height and width for the newborn were taken from the data given in [23]. The values for the adult were determined by averaging the data given in several scientific reports [24–28]. The values for the remaining ages, due to the absence of the data, were derived by linearly interpolating the values between the newborn and adult. For the interpolation, the adult values were assumed to be the same for 18 years of age, considering that the shape of the thyroid gland hardly changes after reaching young adulthood [25,28,29].

The thyroid models were merged with all the other organs/tissues of the pediatric MRCPs that had been constructed [11] and then placed on the typical position of the thyroid, i.e., in front of the second and third tracheal cartilage [17,18]. Finally, the depth of the thyroid gland beneath the skin, i.e., the overlying tissue thickness, was matched to the target values presented in Table 1 by adjusting the skin near the front neck. The adjustment for the newborn, however, was not performed due to the absence of data and even due to the lack of the available space where other organs and tissues adjacent to the thyroid (e.g., clavicles) are already compactly occupied.

2.3. Monte Carlo dose calculations

Using the pediatric MRCPs incorporated with the improved thyroid models, we conducted Monte Carlo (MC) dose calculations for some example cases of external and internal photon exposures. The calculated results were then compared with those calculated with the pediatric VRCPs to investigate a potential dosimetric impact of the present work. We employed a general-purpose MC radiation transport code, Geant4 (GEometry ANd Tracking) [30]. In the Geant4 code (ver. 10.06.p02), the pediatric MRCPs in the TM format and the pediatric VRCPs were implemented via the *G4Tet* class [31] and the *G4NestedParameterised* class [32], respectively. The implemented phantoms were assumed to be in a vacuum. For external exposures, an absorbed dose to the thyroid was calculated by simulating a monoenergetic broad-parallel photon beam for three idealized irradiation geometries (antero-posterior, AP, postero-anterior, PA, and isotropic, ISO) with nineteen energies ranging from 0.01 to 10^4 MeV. As an example, Fig. 3(a) shows the 5-year-old male MRCP and VRCP phantoms implemented in Geant4
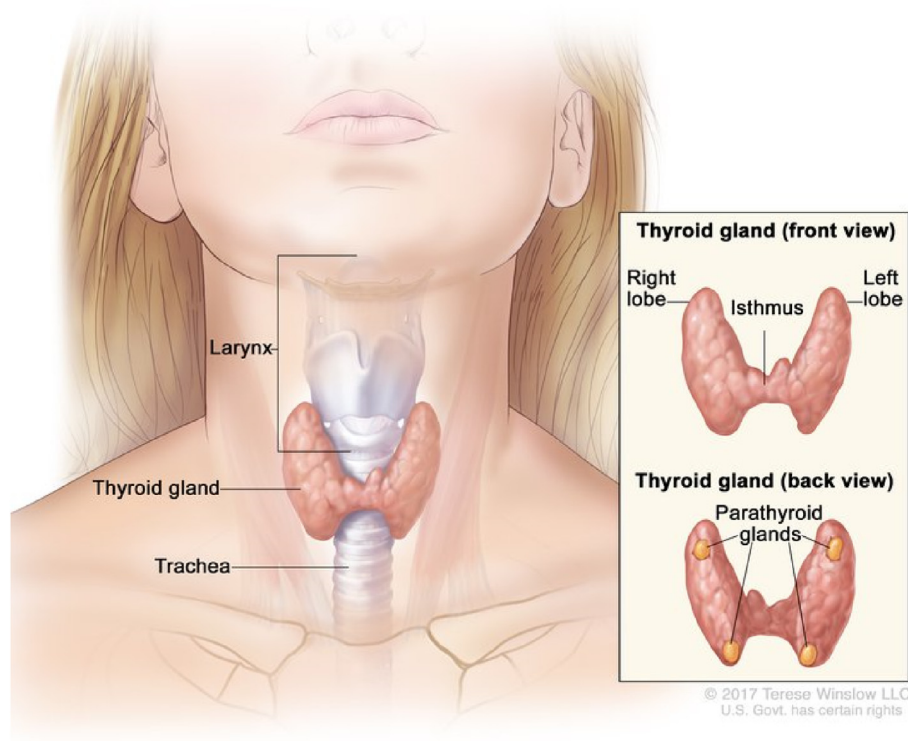
Fig. 1. Anatomical drawing showing the typical location of the thyroid (the copyright of this figure is retained by Terese Winslow, https://visualsonline.cancer.gov/).
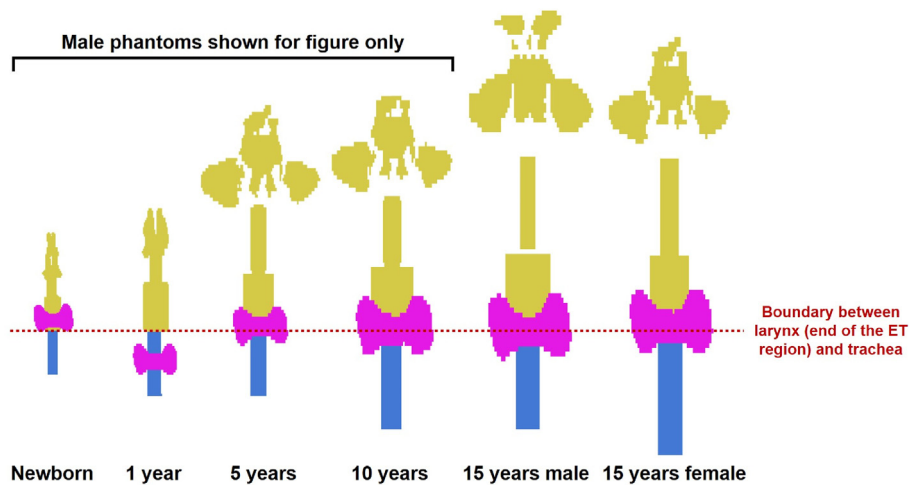
Fig. 2. Thyroids (magenta color) of the pediatric VRCPs with the extrathoracic (ET) region (yellow color) and trachea (blue color). (For interpretation of the references to color in this figure legend, the reader is referred to the Web version of this article.)

and irradiated by 1-MeV photon beams for AP geometry. For internal exposures, a SAF (target ← thyroid) was calculated by simulating a monoenergetic photon uniformly emitted from the thyroid with ten energies ranging from 0.01 to 10 MeV. As an example, Fig. 3(b) also shows the 5-year-old male MRCP and VRCP phantoms implemented in Geant4 where 1-MeV photons were uniformly emitted from the thyroid of the phantoms. The energy deposited to each organ/tissue was calculated via *the G4PSEnergyDeposit* class. Exceptions were the skeletal tissues (i.e., red bone marrow and endosteum), the absorbed doses of which were calculated by using the fluence-to-dose conversion factors established based on micro-CT images and used in ICRP *Publication 144* [33]. We transported 10^7 to 10^{10} primary photons, depending on

the calculation cases to keep statistical errors of the calculated results below 5%. To transport photons and secondary electrons, we used the physics library of *G4EmLivermorePhysics* with a secondary production range cut value of 1 μm.

3. Results and discussion

3.1. Thyroid models for pediatric MRCPs

Fig. 4 shows the thyroid models of the pediatric MRCPs along with those of the pediatric VRCPs. It can be seen that the MRCP thyroid models preserve the general shape of the original voxel thyroid models. It is not clearly observed but the thyroid models

Table 1
Thyroid overlying tissue thickness for the pediatric VRCPs with the age-dependent typical values derived from Likhtarev et al. [19].

		Newborn		1 year		5 years		10 years		15 years	
		Male	Female	Male	Female	Male	Female	Male	Female	Male	Female
Thyroid overlying tissue thickness (mm)	Pediatric VRCPs	8.0	8.0	23.9	23.9	7.7	7.7	1.0	1.0	3.8	1.2
	Typical values	[a]		5.2		5.3		5.5		5.7	

[a] The age range of subjects considered for the measurement of the thyroid overlying tissue thickness is from 1 year to 18 years. As far as we are aware, such data for the newborn do not exist.

Table 2
Reference values of the thyroid mass inclusive of the intra-organ blood mass for the pediatric MRCPs.

	Newborn		1 year		5 years		10 years		15 years	
	Male	Female	Male	Female	Male	Female	Male	Female	Male	Female
Thyroid mass (g)	1.49	1.49	1.97	1.97	3.87	3.87	9.02	9.02	14.04	13.50

Table 3
Target isthmus height, width, and thickness of the thyroid determined for the pediatric MRCPs.

	Newborn	1 year	5 years	10 years	15 years
Isthmus height (mm)	8.6	8.9	10.2	11.8	13.5
Isthmus width (mm)	9.2	9.5	10.4	11.5	12.6
Isthmus thickness (mm)	1.5	1.5	2.0	3.0	3.0

were enlarged to match the blood-inclusive reference values given in Table 2, with the deviations below 0.1%. In addition, the height, width, and thickness of the isthmus for the thyroid mesh models are now in accordance with the target values in Table 3. The deviations are below 3%. Fig. 5 shows the location of the thyroid models in the pediatric MRCPs, which generally well represents the typical location of the thyroid (in front of the second and third tracheal cartilages) shown in Fig. 1. Table 4 shows the overlying tissue thicknesses of the thyroid for the pediatric MRCPs, showing all the values except for the newborn are matched to the target values given in Table 1. Again, note that the overlying tissue for the newborn was not able to be adjusted because the data do not exist and the space between the thyroid and the skin was already compactly filled with other organs/tissues.

3.2. Dosimetry impact for external exposures

To investigate dosimetry impact of the present work, the thyroid doses for the pediatric MRCPs were compared to those of the pediatric VRCPs for photon external exposures in the AP, PA, and ISO geometries. Fig. 6 shows ratios of the thyroid doses of the MRCPs and VRCPs. In the PA geometry, the ratios tend to be very close to the unity over the entire energy region, mostly ranging from 0.90 to 1.10 (i.e., the differences < 10%). Relatively large differences are seen only at the lowest energy (0.02 MeV) where the thyroid doses of the 10- and 15-year-old female MRCPs are lower by 30% and 40%, respectively. In the AP and ISO geometries, the ratios also tend to be very close to the unity at the energies $\geq$ 0.05 MeV; mostly, the differences are again less than 10%. At the lower energies, on the other hand, the ratios tend to largely deviate from the unity. The thyroid doses of the pediatric MRCPs are generally seen to be lower than those of the pediatric VRCPs by up to a factor of 88 (male newborn at 0.01 MeV in AP). Exceptionally, the thyroid doses of the 1-year-old MRCP are greater by two orders of the magnitude at 0.01 MeV in the AP geometry. This is mainly because the overlying tissue thickness of the thyroid for the 1-year-old MRCP (= 4.9 mm on average) is well consistent with the typical values (= 5.2 mm),
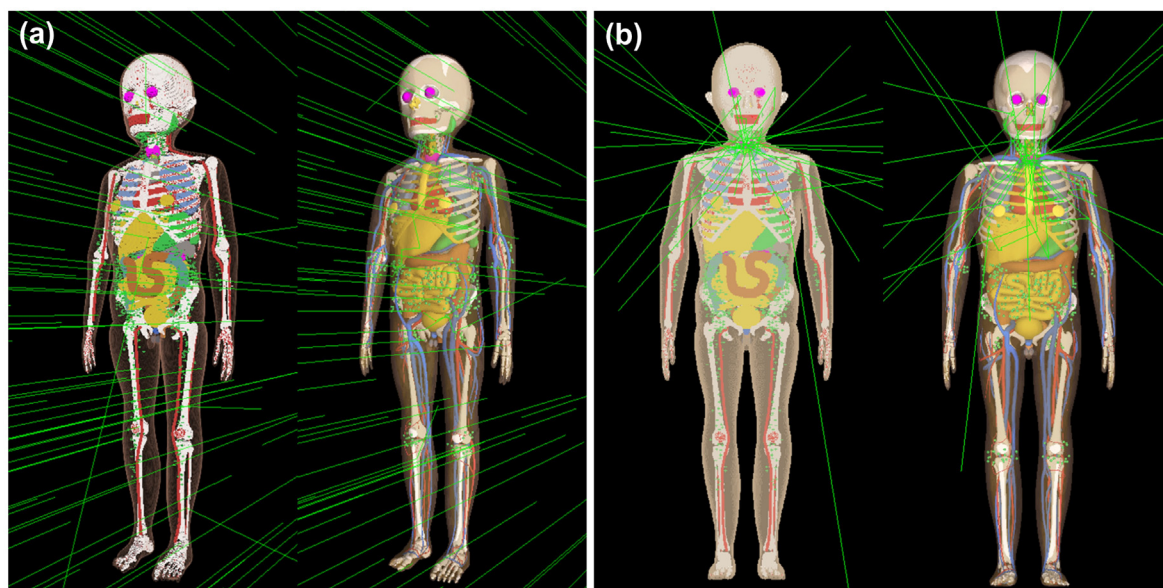
Fig. 3. 5-year-old male VRCP (left) and MRCP (right) phantoms (a) externally irradiated by 1-MeV photons in AP geometry and (b) internally irradiated by 1-MeV photons uniformly emitted from the thyroid.

Y.S. Yeom, C. Choi, B. Shin et al.
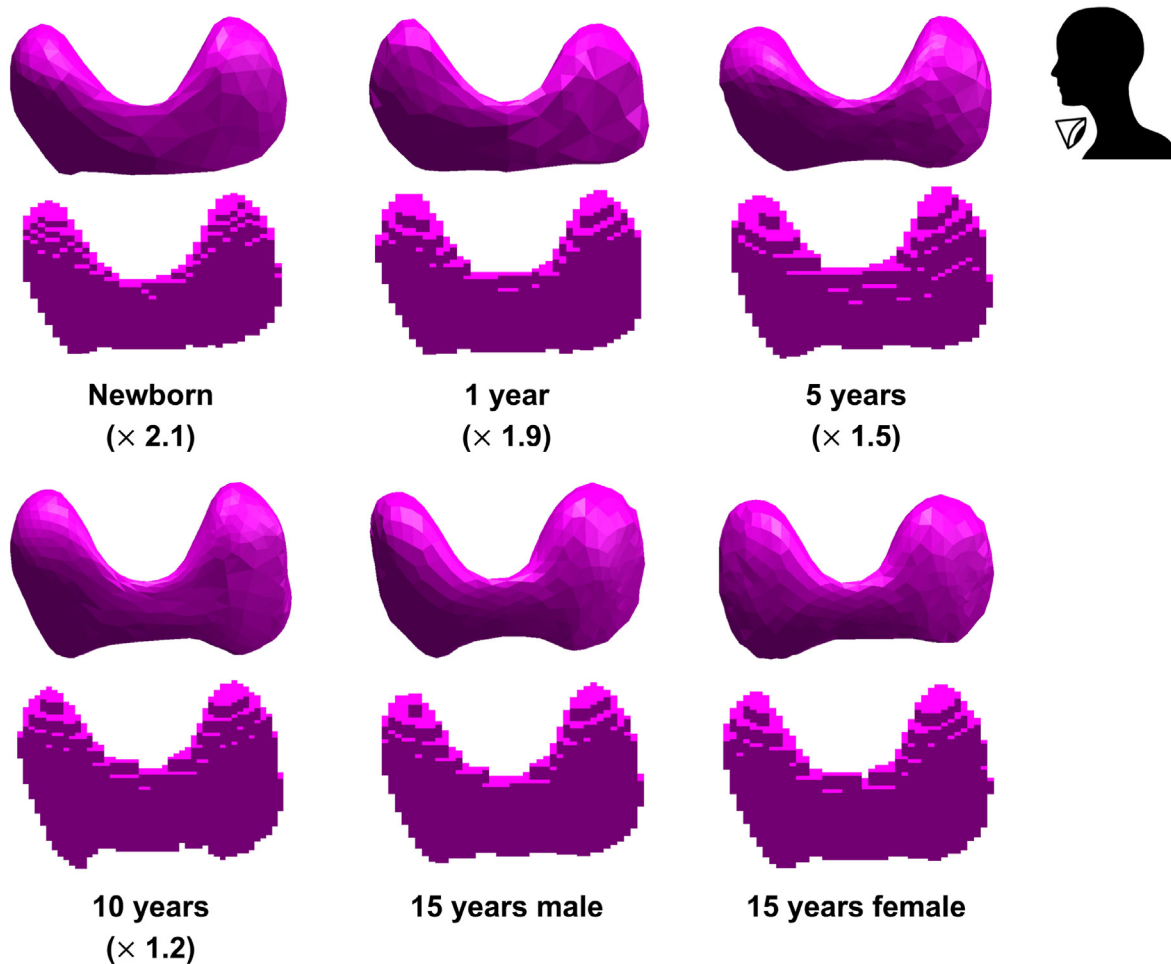
Fig. 4. Developed thyroids of the pediatric MRCPs (upper) along with those of the pediatric VRCPs (lower). For ages up to and including 10 years, only thyroids of the female phantoms are shown.
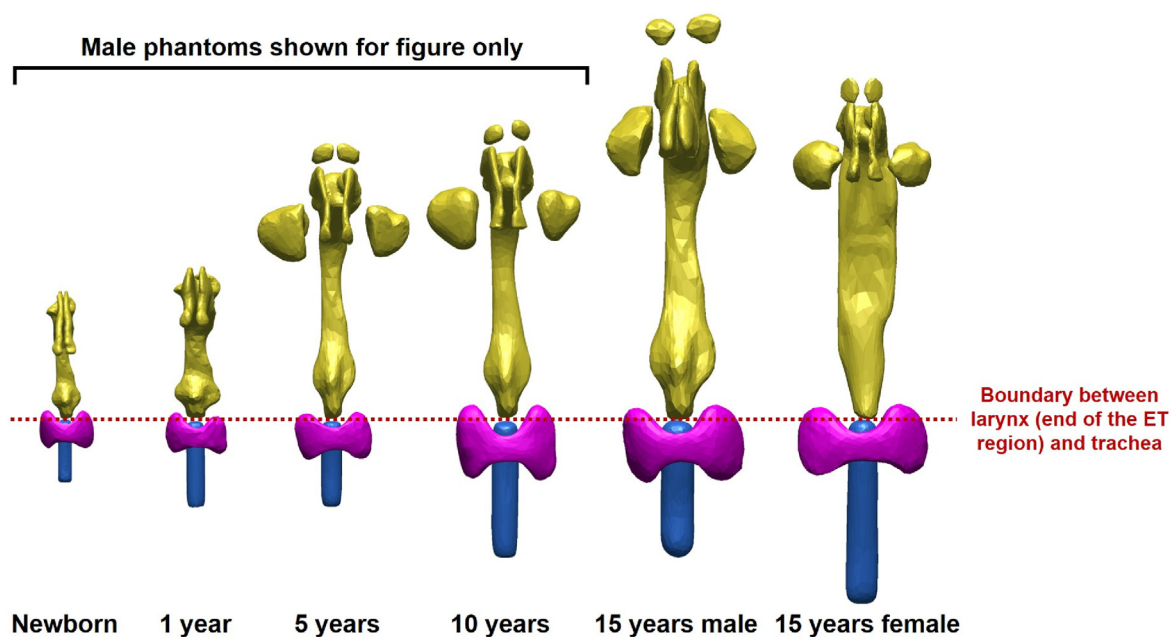
Fig. 5. Thyroids (magenta color) of the pediatric MRCPs with the extrathoracic (ET) region (yellow color) and trachea (blue color). (For interpretation of the references to color in this figure legend, the reader is referred to the Web version of this article.)

Table 4
Thyroid overlying tissue thickness for the pediatric MRCPs.

	Newborn		1 year		5 years		10 years		15 years	
	Male	Female	Male	Female	Male	Female	Male	Female	Male	Female
Thyroid overlying tissue thickness (mm)	11.7	13.2	4.8	5.0	5.1	5.0	5.2	5.1	5.6	5.7
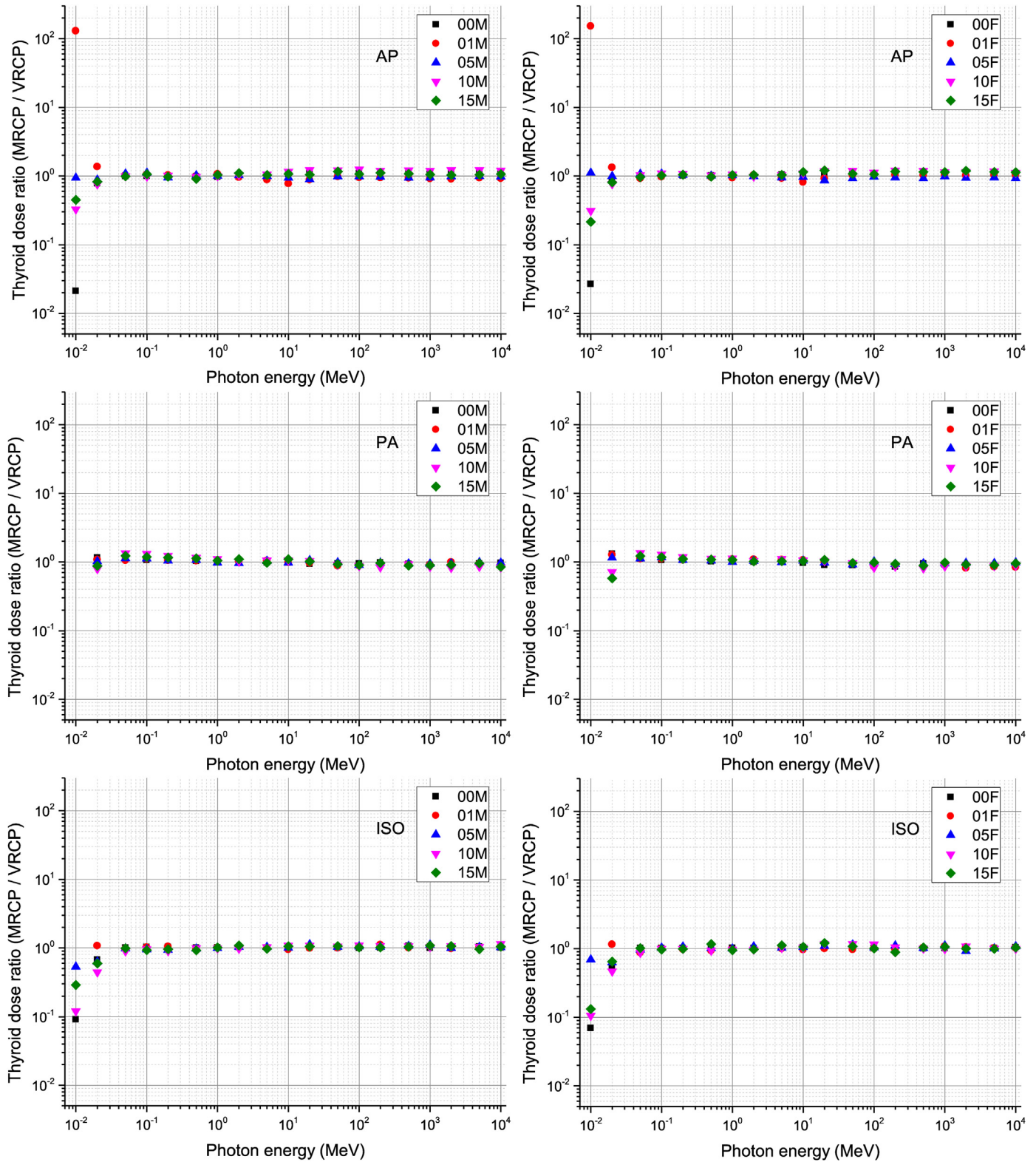
Fig. 6. Ratios of thyroid doses for pediatric mesh-type reference computational phantoms (MRCPs) to those for pediatric voxel-type reference computational phantoms (VRCPs) resulting from whole-body external exposures by a monoenergetic parallel photon beam at three idealized geometries (i.e., antero-posterior, AP; postero-anterior, PA; and isotropic, ISO); male (left) and female (right).
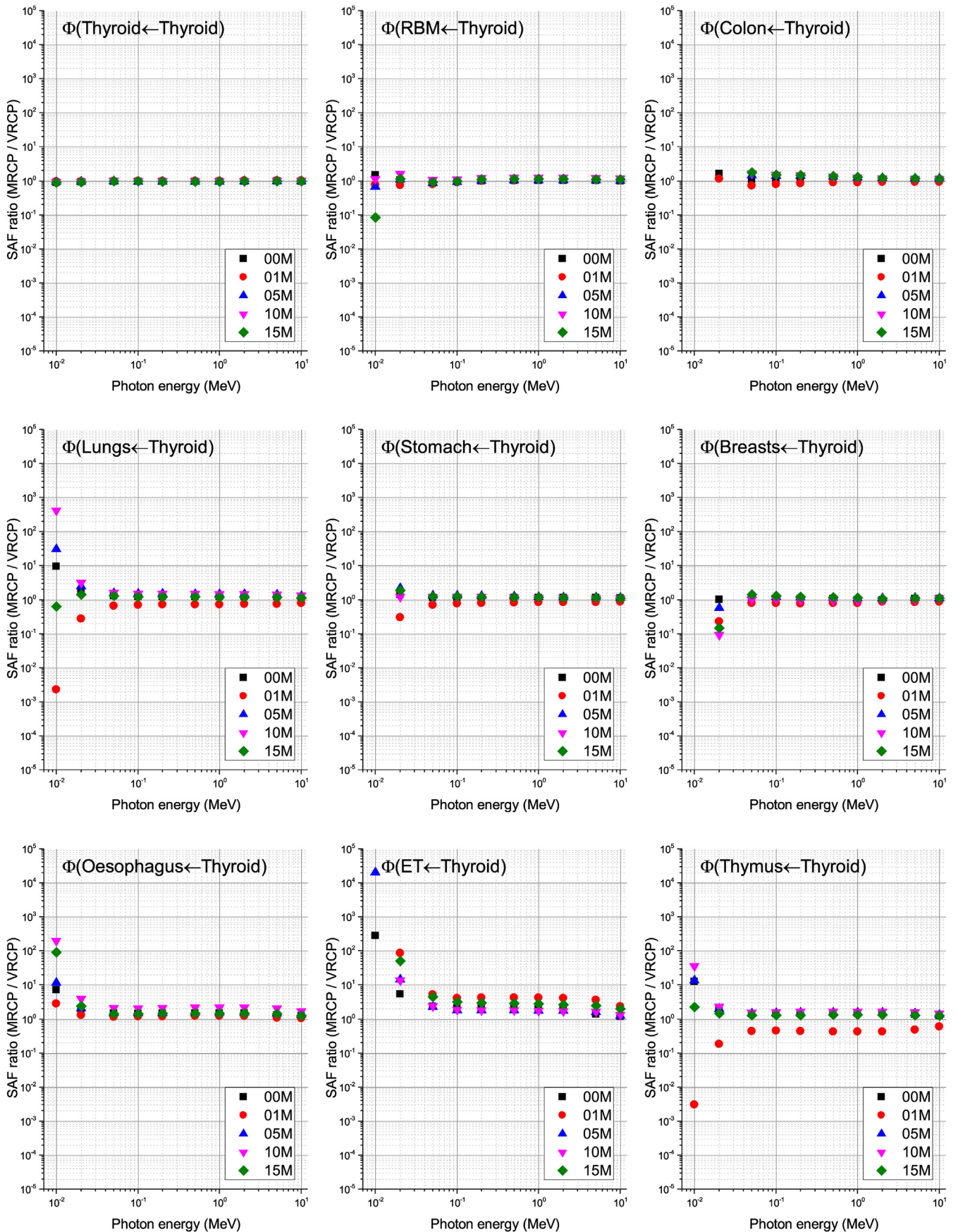
Fig. 7. Ratios of photon SAFs (target ← thyroid) for male pediatric mesh-type reference computational phantoms (MRCPs) to those for male pediatric voxel-type reference computational phantoms (VRCPs) for nine target organs/tissues: thyroid, red bone marrow (RBM), colon, lungs, stomach, breasts, oesophagus, ET, and thymus. (For interpretation of the references to color in this figure legend, the reader is referred to the Web version of this article.)
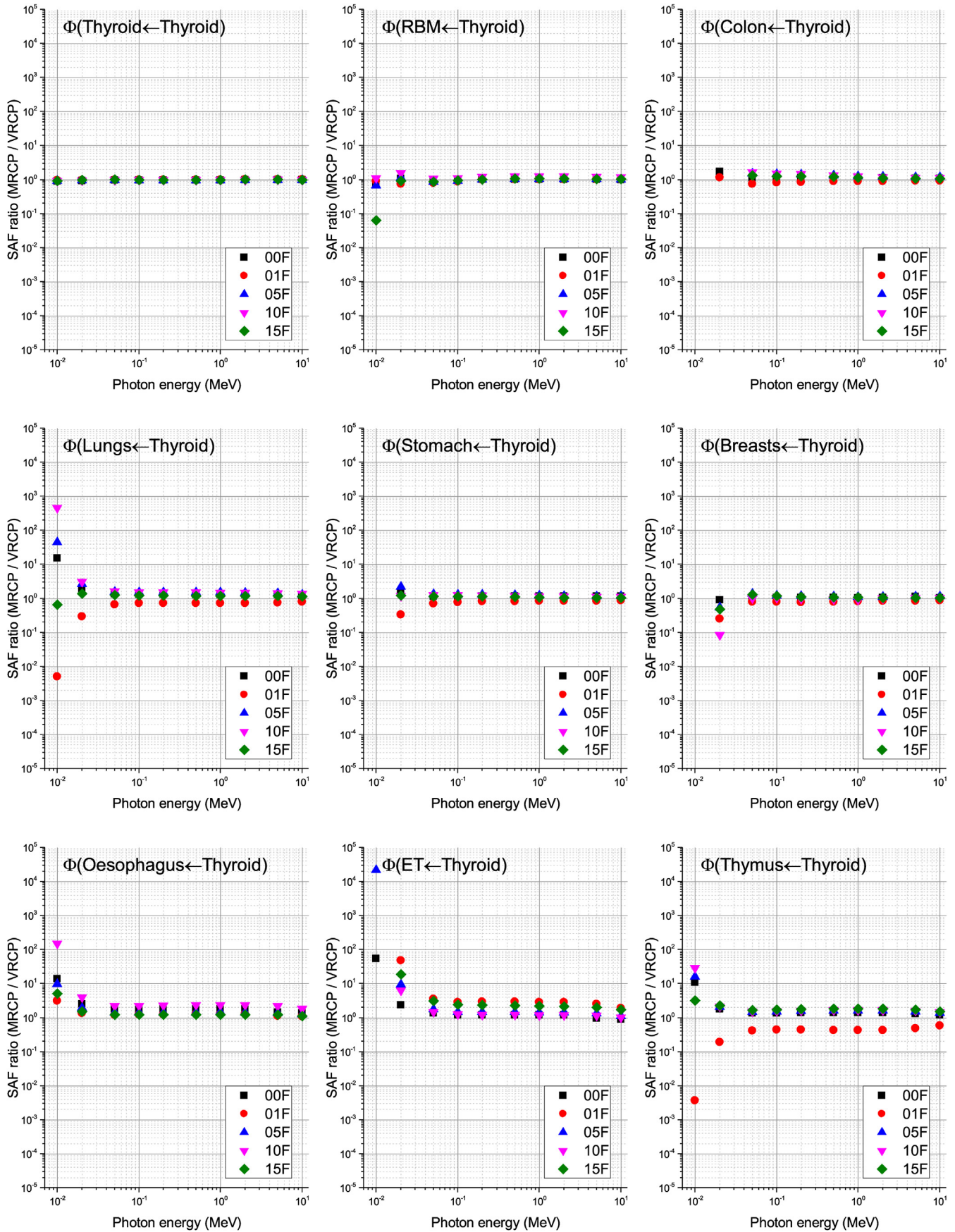
Fig. 8. Ratios of photon SAFs (target ← thyroid) for female pediatric mesh-type reference computational phantoms (MRCPs) to those for female pediatric voxel-type reference computational phantoms (VRCPs) for nine target organs/tissues: thyroid, red bone marrow (RBM), colon, lungs, stomach, breasts, oesophagus, ET, and thymus. (For interpretation of the references to color in this figure legend, the reader is referred to the Web version of this article.)

while that for the 1-year-old VRCP (= 23.9 mm on average) is not (see Table 1). Overall, it can be concluded that the dosimetric impact of the pediatric MRCPs against the pediatric VRCPs is relatively small except for very low energies (<0.03 MeV).

3.3. Dosimetry impact for internal exposures

To investigate the dosimetric impact for internal exposures, we calculated and compared the SAF (target ← thyroid) values between the pediatric MRCPs and VRCPs for nine target organs/tissues: thyroid, red bone marrow (RBM), colon, lungs, stomach, breast, oesophagus, extrathoracic region (ET), and thymus. The RBM, colon, lungs, stomach, and breast are considered by the recent ICRP recommendations [3] as the most radiosensitive at risk of stochastic effects, having the highest tissue weighting factor (= 0.12). The oesophagus, ET, and thymus are the ones which are close to the thyroid.

Fig. 7 shows ratios of the male MRCP SAFs to the male VRCP SAFs for the nine target organs/tissues. For self-irradiation (i.e., SAF (thyroid ← thyroid)), it can be observed that the ratios are close to the unity over the entire energy region (i.e., the differences < 10%). Note that the photon SAFs for self-irradiation is highly dependent on the target mass especially for very low energies [34] and the difference in the thyroid mass between the pediatric MRCPs and VRCPs is not significant (i.e., about 10%). For cross-fire irradiation, on the other hand, the ratios show the largest differences from the unity at the lowest energy, i.e., the largest difference in the SAFs between the MRCPs and VRCPs. For example, the ratio for the SAF (ET ← thyroid) for the 5-year male at 0.01 MeV is ~21,000, which means that the MRCP SAF is greater than the VRCP SAF by a factor of ~21,000. On the other hand, the ratios tend to be closer to the unity with increasing the energy. The ratio for the SAF (ET ← thyroid) for the 5-year male becomes significantly smaller as the energy increases, approaching to ~1.2 at the highest energy (10 MeV). It can be therefore concluded that the dosimetric impact of the pediatric MRCPs against the pediatric VRCPs for the internal photon exposure is generally very large at low energies (below 0.05 MeV) but becomes much smaller at higher energies. We have reached the same conclusion for the female phantoms (see Fig. 8).

It can be also generally seen that the differences in the SAF (target ← thyroid) for the target organs/tissues (e.g., thymus) close to the thyroid tend to be greater than those for the target organs/tissues (e.g., colon) distant from the thyroid. The similar observation was also found in a previous study [35]. Note that the SAF (target ← thyroid) for the target organs/tissues close to the thyroid is contributed mainly by the primary photons emitted from the thyroid which is strongly influenced by the inverse-square-law of radiation field. For the target organs/tissues distant from the thyroid, on the other hand, the SAF contribution by the primary photons becomes less important whereas the contribution by the scattered and secondary photons, which are less influenced by the inverse-square-law, becomes more important.

The result of the SAFs (thymus ← thyroid) as shown in Figs. 7 and 8 is a typical example for a target organ/tissue very close to the thyroid. The MRCP SAFs (thymus ← thyroid) for all the ages only with one exception are greater than the VRCP SAFs by a factor of ~1.2−~36 because the MRCP thyroids were dragged down to be placed in the typical positions (see Figs. 2 and 5) and became closer to the thymus than the VRCP thyroids. The exception is the 1-year-old MRCP SAFs, which are lower than the VRCP SAFs by a factor ~1.7 to ~327, because the thyroid for the 1-year-old MRCPs was dragged up and became more distant from the thymus (see Figs. 2 and 5).

Considering that the ET is also a thyroid's close neighbor in an opposite location to the thymus, the comparison of the SAFs (ET ← thyroid) between the MRCPs and VRCPs could be naturally expected to show an opposite trend of the SAFs (thymus ← thyroid). The expected trend, however, cannot be observed in the result of the SAFs (ET ← thyroid) as shown in Figs. 7 and 8. The MRCP SAFs (ET ← thyroid) regardless of the age are generally greater than the VRCP SAFs, which cannot be explained by the adjusted location of the MRCP thyroids in the present work. The greater values of the MRCP SAFs (ET ← thyroid) were due mainly to the anatomical enhancement of the ET for the MRCPs against the VRCPs [11]. While the ET consists of the ET_1 (anterior nose) and ET_2 (posterior nasal passages, pharynx, and larynx) described in ICRP *Publication 66* [6], the larynx was included not in the ET_2 but in cartilage when modifying the UF/NCI pediatric phantoms [15] to the pediatric VRCPs [1]. This limitation resulted in the unreasonably longer distances between the ET and thyroid for the pediatric VRCPs, which was addressed in the pediatric MRCPs [11].

4. Conclusion

In the present study, we constructed the thyroid models for the pediatric MRCPs, which are currently under development by the ICRP Task Group 103 and will be considered as the new ICRP pediatric reference phantoms over the current VRCPs in ICRP *Publication 143* [1]. The pediatric MRCP thyroid models were constructed by converting the pediatric VRCP thyroid models to a high-quality mesh format, faithfully maintaining the original shape but also improving several anatomical parameters of the thyroid (e.g., mass, overlying tissue thickness, and location). We investigated the dosimetric impact due mainly to the development of the new thyroid models for the pediatric MRCPs for some external and internal exposures to photons, finding that the thyroid doses between the MRCPs and VRCPs are not significantly different for the external exposures except for very low energies (<0.03 MeV). On the other hand, significant differences in photon SAFs (target ← thyroid) between the MRCPs and VRCPs especially for the target organs/tissues very close to the thyroid (e.g., thymus) were frequently observed due mainly to the anatomical improvement of the thyroid models. Although limited exposure cases were considered in the present work mainly focusing on the development of the pediatric MRCP thyroid models, we believe that the pediatric MRCPs may provide more reliable dose values in other exposure cases when the thyroid is a source and/or target region.

Declaration of competing interest

The authors declare that they have no known competing financial interests or personal relationships that could have appeared to influence the work reported in this paper.

Acknowledgments

References

[1] ICRP, Paediatric reference computational phantoms, ICRP Publication 143, Ann. ICRP 49 (2020) 5−297, https://doi.org/10.1177/0146645320915031.

[2] ICRP, Adult reference computational phantoms, ICRP Publication 110, Ann. ICRP 39 (2009) 1−165.

[3] ICRP, The 2007 recommendations of the international commission on radiological protection, ICRP Publication 103, Ann. ICRP 37 (2007) 1−332.

[4] ICRP, Recommendations of the international commission on radiological protection, ICRP publication 26, Ann. ICRP 1 (1977) 1−53.

[5] ICRP, Recommendations of the international commission on radiological protection, ICRP publication 60, Ann. ICRP 21 (1991) (1990) 1−201.

[6] ICRP, Human respiratory tract model for radiological protection, ICRP publication 66, Ann. ICRP 24 (1994) 1−482.

[7] ICRP, Human alimentary tract model for radiological protection, ICRP publication 100, Ann. ICRP 36 (2006) 1−336.

[8] ICRP, The ICRP computational framework for internal dose assessment for reference adults: specific absorbed fractions, ICRP publication 133, Ann. ICRP 45 (2016) 5−73, https://doi.org/10.1177/0146645316661077.

[9] C.H. Kim, Y.S. Yeom, T.T. Nguyen, M.C. Han, C. Choi, H. Lee, H. Han, B. Shin, J.-K. Lee, H.S. Kim, M. Zankl, N. Petoussi-Henss, W.E. Bolch, C. Lee, B.S. Chung, R. Qiu, K. Eckerman, New mesh-type phantoms and their dosimetric applications, including emergencies, Ann. ICRP 47 (2018) 45−62, https://doi.org/10.1177/0146645318756231.

[10] ICRP, Adult mesh-type reference computational phantoms, ICRP publication 145, Ann. ICRP 49 (2020) 13−201, https://doi.org/10.1177/0146645319893605.

[11] C. Choi, B. Shin, Y.S. Yeom, T.T. Nguyen, H. Han, S. Ha, B.S. Chung, W.E. Bolch, C.H. Kim, Development of paediatric mesh-type reference computational phantom series of international commission on radiological protection, J. Radiol. Prot. 41 (2021) S160−S170, https://doi.org/10.1088/1361-6498/ac0801.

[12] L.B. Zablotska, E. Ron, A.V. Rozhko, M. Hatch, O.N. Polyanskaya, A.V. Brenner, J. Lubin, G.N. Romanov, R.J. McConnell, P. O'Kane, V.V. Evseenko, V.V. Drozdovitch, N. Luckyanov, V.F. Minenko, A. Bouville, V.B. Masyakin, Thyroid cancer risk in Belarus among children and adolescents exposed to radioiodine after the chornobyl accident, Br. J. Cancer 104 (2011) 181−187, https://doi.org/10.1038/sj.bjc.6605967.

[13] A.V. Brenner, M.D. Tronko, M. Hatch, T.I. Bogdanova, V.A. Oliynik, J.H. Lubin, L.B. Zablotska, V.P. Tereschenko, R.J. Mcconnell, G.A. Zamotaeva, P. O'Kane, A.C. Bouville, L.V. Chaykovskaya, E. Greenebaum, I.P. Paster, V.M. Shpak, E. Ron, I-131 dose response for incident thyroid cancers in Ukraine related to the Chornobyl accident, Environ. Health Perspect. 119 (2011) 933−939, https://doi.org/10.1289/ehp.1002674.

[14] M.D. Tronko, G.R. Howe, T.I. Bogdanova, A.C. Bouville, O.V. Epstein, A.B. Brill, I.A. Likhtarev, D.J. Fink, V.V. Markov, E. Greenebaum, V.A. Olijnyk, I.J. Masnyk, V.M. Shpak, R.J. McConnell, V.P. Tereshchenko, J. Robbins, O.V. Zvinchuk, L.B. Zablotska, M. Hatch, N.K. Luckyanov, E. Ron, T.L. Thomas, P.G. Voillequé, G.W. Beebe, A cohort study of thyroid cancer and other thyroid diseases after the chornobyl accident: thyroid cancer in Ukraine detected during first screening, J. Natl. Cancer Inst. 98 (2006) 897−903, https://doi.org/10.1093/jnci/djj244.

[15] C. Lee, D. Lodwick, J. Hurtado, D. Pafundi, J.L. Williams, W.E. Bolch, The UF family of reference hybrid phantoms for computational radiation dosimetry, Phys. Med. Biol. 55 (2010) 339−363, https://doi.org/10.1088/0031-9155/55/2/002.

[16] ICRP, Basic anatomical and physiological data for use in radiological protection reference values, ICRP publication 89, Ann. ICRP 32 (2002) 1−277.

[17] H. Ellis, Anatomy of the thyroid and parathyroid glands, Surgery (Oxford) 25 (2007) 467−468, https://doi.org/10.1016/j.mpsur.2007.09.011.

[18] B.F. Naqshi, S. Seth, A.B. Shah, S. Gupta, S. Raina, Thyroid hemiagenesis with agenesis of isthmus a case report, J. Med. Sci. Clin. Res. 4 (2016) 10799−10801, https://doi.org/10.18535/jmscr/v4i6.19.

[19] I.A. Likhtarev, G.M. Gulko, B.G. Sobolev, I.A. Kairo, G. Pröhl, P. Roth, K. Henrichs, G.M. Grulko, Evaluation of the 131I thyroid-monitoring measurements performed in Ukraine during May and June of 1986, Health Phys. 69 (1995) 6−15, https://doi.org/10.1097/00004032-199507000-00002.

[20] C.H. Kim, J.H. Jeong, W.E. Bolch, K.W. Cho, S.B. Hwang, A polygon-surface reference Korean male phantom (PSRK-Man) and its direct implementation in Geant4 Monte Carlo simulation, Phys. Med. Biol. 56 (2011) 3137−3161,

https://doi.org/10.1088/0031-9155/56/10/016.

[21] Y.S. Yeom, M.C. Han, C.H. Kim, J.H. Jeong, Conversion of ICRP male reference phantom to polygon-surface phantom, Phys. Med. Biol. 58 (2013) 6985−7007, https://doi.org/10.1088/0031-9155/58/19/6985.

[22] J.H. Sea, H. Ji, S.K. You, J.E. Lee, S.M. Lee, H.H. Cho, Age-dependent reference values of the thyroid gland in pediatric population; from routine computed tomography data, Clin. Imaging 56 (2019) 88−92, https://doi.org/10.1016/j.clinimag.2019.04.001.

[23] G. Ozguner, O. Sulak, Size and location of thyroid gland in the fetal period, Surg. Radiol. Anat. 36 (2014) 359−367, https://doi.org/10.1007/s00276-013-1177-2.

[24] E.C.K. Tong, S. Rubenfeld, Scan measurements of normal and enlarged thyroid glands, Am. J. Roentgenol. Radium Ther. Nucl. Med. 115 (1972) 706−708, https://doi.org/10.2214/ajr.115.4.706.

[25] A. Harjeet, D. Sahni, I. Jit, A.K. Aggarwal, Shape, measurements and weight of the thyroid gland in northwest Indians, Surg. Radio. Anat. 26 (2004) 91−95, https://doi.org/10.1007/s00276-003-0194-y.

[26] S.D. Joshi, S.S. Joshi, S.R. Daimi, S.A. Athavale, The thyroid gland and its variations: a cadaveric study, Folia Morphol. 69 (2010) 47−50.

[27] Z. Ozgur, S. Celik, F. Govsa, T. Ozgur, Anatomical and surgical aspects of the lobes of the thyroid glands, Eur. Arch. Otorhinolaryngol. 268 (2011) 1357−1363, https://doi.org/10.1007/s00405-011-1502-5.

[28] H.S. Won, S.H. Han, C.S. Oh, H.J. Chung, H.J. Won, J.H. Kim, The location and morphometry of the thyroid isthmus in adult Korean cadavers, Anat. Sci. Int. 88 (2013) 212−216, https://doi.org/10.1007/s12565-013-0187-9.

[29] S.Z. Sultana, M. Khalil, M.K. Khan, M.M. Rahman, S. Mannan, F. Wahed, S. Choudhury, Morphometry of isthmus of thyroid gland in bangladeshi cadaver, Mymensingh Med. J. 20 (2011) 366−370.

[30] J. Allison, K. Amako, J. Apostolakis, P. Arce, M. Asai, T. Aso, E. Bagulya, S. Banerjee, G. Barrand, B.R. Beck, A.G. Bogdanov, D. Brandt, J.M.C. Brown, H. Burkhardt, Ph Canal, D. Cano-Ott, S. Chauvie, K. Cho, G.A.P. Cirrone, G. Gooperman, M.A. Cortés-Giraldo, G. Cosmo, G. Cuttone, G. Depaola, L. Desorgher, X. Dong, A. Dotti, V.D. Elvira, G. Folger, Z. Francis, A. Galoyan, L. Garnier, M. Gayer, K.L. Genser, V.M. Grichine, S. Guatelli, P. Guèye, P. Gumplinger, A.S. Howard, I. Hřivnáčová, S. Hwang, S. Incerti, A. Ivanchenko, V.N. Ivanchenko, F.W. Jones, S.Y. Jun, P. Kaitaniemi, N. Karakatsanis, M. Karamitros, M. Kelsey, A. Kimura, T. Koi, H. Kurashige, A. Lechner, S.B. Lee, F. Longo, M. Maire, D. Mancusi, A. Mantero, E. Mendoza, B. Morgan, K. Murakami, T. Nikitina, L. Pandola, P. Paprocki, J. Perl, I. Petrović, M.G. Pia, W. Pokorski, J.M. Quesada, M. Raine, M.A. Reis, A. Ribon, A. Ristić Fira, F. Romano, G. Russo, G. Santin, T. Sasaki, D. Sawkey, J.I. Shin, I.I. Strakovsky, A. Taborda, S. Tanaka, B. Tomé, T. Toshito, H.N. Tran, P.R. Truscott, L. Urban, V. Uzhinsky, J.M. Verbeke, M. Verderi, B.L. Wendt, H. Wenzel, D.H. Wright, D.M. Wright, T. Yamashita, J. Yarba, H. Yoshida, Recent developments in Geant4, Nucl. Instrum. Methods Phys. Res. Sect. A Accel. Spectrom. Detect. Assoc. Equip. 835 (2016) 186−225, https://doi.org/10.1016/j.nima.2016.06.125.

[31] Y.S. Yeom, J.H. Jeong, M.C. Han, C.H. Kim, Tetrahedral-mesh-based computational human phantom for fast Monte Carlo dose calculations, Phys. Med. Biol. 59 (2014) 3173−3185, https://doi.org/10.1088/0031-9155/59/12/3173.

[32] J. Schümann, H. Paganetti, J. Shin, B. Faddegon, J. Perl, Efficient voxel navigation for proton therapy dose calculation in TOPAS and Geant4, Phys. Med. Biol. 57 (2012) 3281−3293, https://doi.org/10.1088/0031-9155/57/11/3281.

[33] ICRP, Dose coefficients for external exposures to environmental sources, ICRP publication 144, Ann. ICRP 49 (2020) 11−145, https://doi.org/10.1177/0146645320906277.

[34] M. Zankl, N. Petoussi-Henss, U. Fill, D. Regulla, The application of voxel phantoms to the internal dosimetry of radionuclides, Radiat. Prot. Dosim. 105 (2003) 1−4, https://doi.org/10.1093/oxfordjournals.rpd.a006299.

[35] Y.S. Yeom, K. Griffin, B. Shin, C. Choi, H. Han, S. Moon, Body-size-dependent iodine-131 S values, J. Radiol. Prot. 40 (2020) 1311−1320, https://doi.org/10.1088/1361-6498/abc053.